Taylor & Francis
Taylor & Francis Group

Phase Transitions
A Multinational Journal

ISSN: (Print) (Online) Journal homepage: https://www.tandfonline.com/loi/gpht20

Physical and electrochemical properties of spray-deposited Co_3O_4 thin films

Abhijit A. Yadav

To cite this article: Abhijit A. Yadav (2021) Physical and electrochemical properties of spray-deposited Co_3O_4 thin films, Phase Transitions, 94:10, 691-704, DOI: 10.1080/01411594.2021.1965602

To link to this article: https://doi.org/10.1080/01411594.2021.1965602

PHASE TRANSITIONS
2021, VOL. 94, NO. 10, 691–704
https://doi.org/10.1080/01411594.2021.1965602

Taylor & Francis
Taylor & Francis Group

Physical and electrochemical properties of spray-deposited Co_3O_4 thin films

Abhijit A. Yadav

Thin Film Physics Laboratory, Department of Physics, Electronics and Photonics, Rajarshi Shahu Mahavidyalaya (Autonomous), Latur, India

ABSTRACT

Nanostructured cobalt oxide films have been prepared by a simple and cost-effective chemical spray pyrolysis. The effect of the quantity of the spraying solution for various film properties has been studied. The X-ray diffraction analysis shows that Co_3O_4 thin films are cubic in nature with strong (311) orientation. SEM images show a porous morphology. Optical band gap energies are between 1.41 and 1.48 eV in the lower and 1.84–2.02 eV in the higher energy regions, respectively. Specific capacitance is 565 Fg^{-1} at a scan rate of 5 mVs^{-1}. Specific energy 57.50 $Whkg^{-1}$, specific power 1.8 $kWkg^{-1}$ and columbic efficiency 89.15% are found from galvanostatic charge/discharge studies. Such unique nanostructures delivered adequate active sites for redox reaction resulting in enhanced electrochemical behaviour. These findings suggest a favourable route towards the fabrication of electrodes for high-performance supercapacitors.

ARTICLE HISTORY
Received 25 May 2021
Accepted 4 August 2021

KEYWORDS
Spray pyrolysis; Co_3O_4; supercapacitor; electrochemical impedance spectroscopy

1. Introduction

Worldwide climate change and greenhouse effect have placed a crucial demand on sustainable and renewable energy sources, such as solar and wind energy in current years [1–5]. Also, the reliable energy storage technologies are of equal significance. Electrochemical energy storage devices, lithium-ion batteries and supercapacitors, offer the possibility to reversibly store electric energy in an economic and efficient manner. Electrochemical supercapacitor is an advanced technology because it seals the gap between batteries and conventional capacitors. Supercapacitors have remarkable characteristics such as high power density than batteries and also high energy density than conventional capacitors [6].

Carbon-based materials, metal oxides and polymers are the best candidates in the development of energy-efficient and cost-effective supercapacitors [3,4,7,8]. Among these, metal oxides are favourable electrode materials due to their high specific capacitance, low resistance, easier in construction with high energy and power density. The most beneficial metal oxide to give high specific capacitance is RuO_2. But it is costly and is available in rare quantities. Therefore, other metal oxides, such as MnO_2, Co_3O_4, NiO, IrO_2, FeO, TiO_2, SnO_2, V_2O_5, and MoO, are studied [4,9]. Out of these, cobalt oxide is one of the most studied oxides due to its applications in various devices. Co_3O_4 can provide good surface area, extraordinary conductivity and worthy electrochemical stability. Also, the literature has shown that Co_3O_4 electrode has good efficiency and long-term performance [10].

Deng et al. [11] fabricated ordered mesoporous spinel Co_3O_4 using the nanocasting. Co_3O_4 displayed superior catalytic performance due to its large specific surface area, high pore volume, and high Co^{2+} content and high density of surface active sites. Patil and coworkers [12] synthesized the

CONTACT Abhijit A. Yadav aay_physics@yahoo.co.in

nanocrystalline spinal Co_3O_4 thin films by the spin coating method. Carrier concentration and the mobility of Co_3O_4 films are 10^{19} cm^{-3} and 10^{-5} $cm^2V^{-1}s^{-1}$, respectively. Pal and colleagues [13] have grown self-supported Co_3O_4 nanocubes over Ni foam by the solvothermal method. These nanocubes exhibited a specific capacitance of 1913 Fg^{-1} at the current density of 8 Ag^{-1} with high rate capability and good cycling stability. Shinde et al. [10] studied supercapacitive performances of spray-deposited cobalt oxides. These films showed a specific capacitance of 74 Fg^{-1}. The use of r.f. sputtered cobalt oxide electrodes in supercapacitors was reported also by Kim et al. [14]. Huang and colleagues [15] synthesized novel porous polyhedral and fusiform Co_3O_4 powders through the hydrothermal method. Jagadale et al. [16] deposited Co_3O_4 thin films via the potentiodynamic electrodeposition method with a specific capacitance of 365 Fg^{-1} in 1M KOH at a scan rate of 5 mVs^{-1}. These and other studies [17–21] indicated that Co_3O_4 thin film electrode is one of the most favourable materials for the supercapacitors. The spray pyrolysis technique is very simple, cost-effective, versatile, environment-friendly and most widely used for the synthesis of semiconductor oxides. There are very little reports on spray-deposited Co_3O_4 thin films using mixed aqueous/organic solvents. Therefore, in the present study, Co_3O_4 thin films are spray-deposited at different quantities of the spraying solution using mixed aqueous/organic solvents and their physical and electrochemical properties are studied.

2. Experimental

Cobalt chloride hexahydrate (0.05M) is taken as a precursor material to prepare Co_3O_4 films. This stock solution with Propan-2-ol (1:1) is used as the precursor solution. Thoroughly cleaned amorphous and FTO-coated glass substrates were used. Nozzle to substrate distance is maintained at 30 cm during all depositions. All the films are deposited at an optimized substrate temperature of 350°C by using the computerized spray pyrolysis technique discussed elsewhere [22]. The quantity of the spraying solution ($CoCl_2.6H_2O$) is varied from 15 to 30 cc at the interval of 5 cc. Atmospheric air was used as the carrier gas. The spray rate employed was 3 $ccmin^{-1}$ and kept constant throughout the depositions.

Spray-deposited films are characterized by XRD, SEM, UV–Vis–NIR Spectra, electrical resistivity and electrochemical measurements. Film thickness is calculated by the gravimetric weight difference method. Structural analysis of the Co_3O_4 thin films is carried out using X-ray diffractometer (wavelength $\lambda = 1.5406$ Å for Cu-Kα radiation). Surface morphology is studied by using a JEOL-JSM-6360A analytical scanning electron microscope. The band gap energy of Co_3O_4 thin films is estimated from the optical absorption studies, using a UV-Vis spectrophotometer. Electrical resistivity measurements are performed using a DC two-point probe method in the temperature range 300–500 K. Electrochemical measurements are carried out in a standard three-electrode cell on a CHI 660E, supplied by CH Instruments, USA, with Co_3O_4 as the working electrode, a Platinum foil counter electrode, and an Ag/AgCl as a reference electrode with 2M aqueous KOH as an electrolyte. Cyclic voltammetry study is performed in a potential range from −0.8 to +0.1 V vs Ag/AgCl at different scan rates. The measurements of electrochemical impedance are taken in the frequency range of 100 kHz –1 Hz.

3. Results and discussion

3.1. Film formation

Cobalt oxide thin films are deposited by varying the quantities of the spraying solution. As deposited, cobalt oxide films appear blackish with uniform surface and strongly adherent to substrates. The apparent reaction mechanism could be inscribed as follows:

$$3CoCl_2 + 2H_2O + O_2 \rightarrow Co_3O_4 \downarrow + 3Cl_2 \uparrow + 2H_2 \uparrow \quad (1)$$

A similar type of reaction mechanism was earlier reported by Shinde et al. [10] for Co_3O_4 thin films deposited by the spray pyrolysis.

The gravimetric weight difference method is used to measure the film thickness. Figure 1 shows the plot of film thickness vs the quantity of the spraying solution. The figure shows that, the film thickness increases with the rise in the quantity of the spraying solution and then saturates. The probable reason for such behaviour is the supply of extra ingredient ions with an increase in the quantity of the spraying solution. Maximum film thickness (415 nm) is obtained for the film deposited by spraying 30 cc of cobaltous chloride. Similar behaviour was earlier reported for the spray-deposited fluorine-doped SnO_2 thin films [23].

3.2. X-ray diffraction studies

Figure 2 shows the XRD patterns of the Co_3O_4 films. Considerable improvement in the film crystallinity is observed with an increase in the quantity of the spraying solution. All the diffraction peaks can be indexed to the standard JCPDS data cards. Diffraction peaks are observed for $2\theta = 19.30°$, 31.54°, 37.18°, 45.09°, 59.72° and 65.31° which are indexed to (111), (220), (311), (400), (511) and (440) reflections of Co_3O_4, which implies that films are polycrystalline. The entire diffraction peaks match well with the cubic phase Co_3O_4 (JCPDS data card no. 76–1802). The calculated average lattice parameter is a = b = c = 8.030 Å, which is slightly less than the standard value of 8.084 Å [24].

Crystalline size (D) is calculated using Scherrer equation [25],

$$D = \frac{k\lambda}{\beta cos\theta} \tag{2}$$

where k is the constant, λ is the wavelength of incident radiation (λ = 1.5406 Å for Cu-K_α radiation) and θ is the Braggs angle. Crystalline size calculated for (311) peak continuously increases from 26 to 32 nm with the increase of the quantity of the spraying solution (Table 1) due to the improved nucleation centres [26]. A similar thickness-dependent behaviour of crystalline size was observed by Giraldi and colleagues [27] for Sb-doped SnO_2 thin films. The values of lattice parameters, miller indices and crystalline size for Co_3O_4 thin films are presented in Table 1.

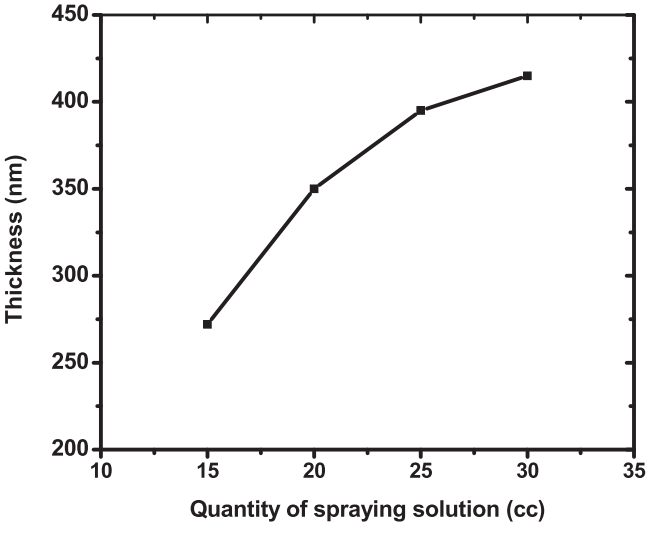

Figure 1. Variation of film thickness with quantity of the spraying solution for spray-deposited Co_3O_4 thin films.

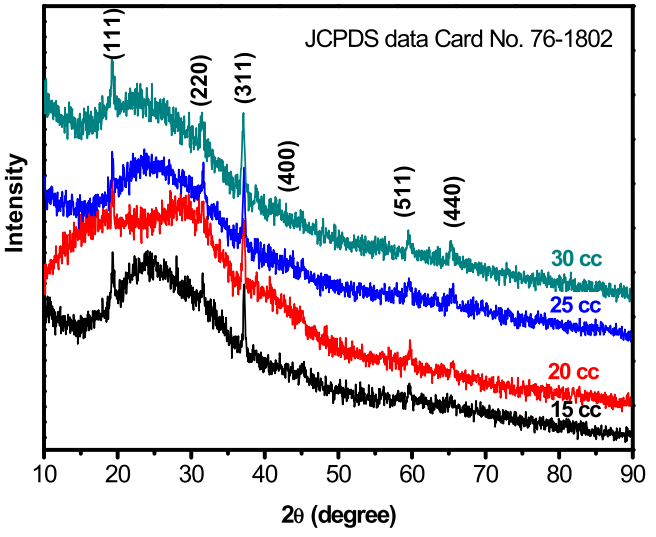

Figure 2. X-ray diffraction patterns of Co_3O_4 films spray-deposited with various quantities of the spraying solution.

3.3. Surface morphology studies

The surface morphology of spray-deposited Co_3O_4 thin films is studied by scanning electron microscopy. Figure 3 shows the SEM images of Co_3O_4 thin films prepared with various quantities of the spraying solution. From SEM images it is perceived that the films present a uniform morphology with small grains and has a heterogeneous surface with a mesoporous structure. No cracks are observed on the film surface. The crystallinity of Co_3O_4 improves and the enhancement in grain size was observed with increasing quantity of the spraying solution. The agglomeration of grains

Table 1. XRD data for Co_3O_4 thin films spray deposited with various quantities of the spraying solution.

Quantity of the spraying solution (cc)	2θ (°)	θ (°)	d (Å) calculated	d (Å) standard	(hkl)	D (nm)
	19.30	9.65	4.5973	4.6604	111	
	31.54	15.77	2.8353	2.8539	220	
15	37.21	18.60	2.4156	2.4338	311	26
	45.01	22.50	2.0136	2.0180	400	
	59.65	29.82	1.5496	1.5535	511	
	65.31	32.66	1.4282	1.4269	440	
	19.28	9.64	4.6022	4.6604	111	
	31.67	15.83	2.8247	2.8539	220	
20	37.17	18.58	2.4182	2.4338	311	28
	45.07	22.53	2.0110	2.0180	400	
	59.73	29.86	1.5477	1.5535	511	
	65.59	32.80	1.4227	1.4269	440	
	19.26	9.63	4.6070	4.6604	111	
	31.67	15.83	2.8247	2.8539	220	
25	37.19	18.59	2.4169	2.4338	311	30
	45.17	22.58	2.0067	2.0180	400	
	59.58	29.79	1.5511	1.5535	511	
	65.61	32.81	1.4223	1.4269	440	
	19.29	9.65	4.5999	4.6604	111	
	31.55	15.78	2.8345	2.8539	220	
30	37.26	18.63	2.4125	2.4338	311	32
	45.11	22.55	2.0093	2.0180	400	
	59.59	29.79	1.5510	1.5535	511	
	65.29	32.65	1.4286	1.4269	440	

θ: Bragg diffraction angle; d: interplanar spacing; (hkl): miller indices; D: crystalline size.

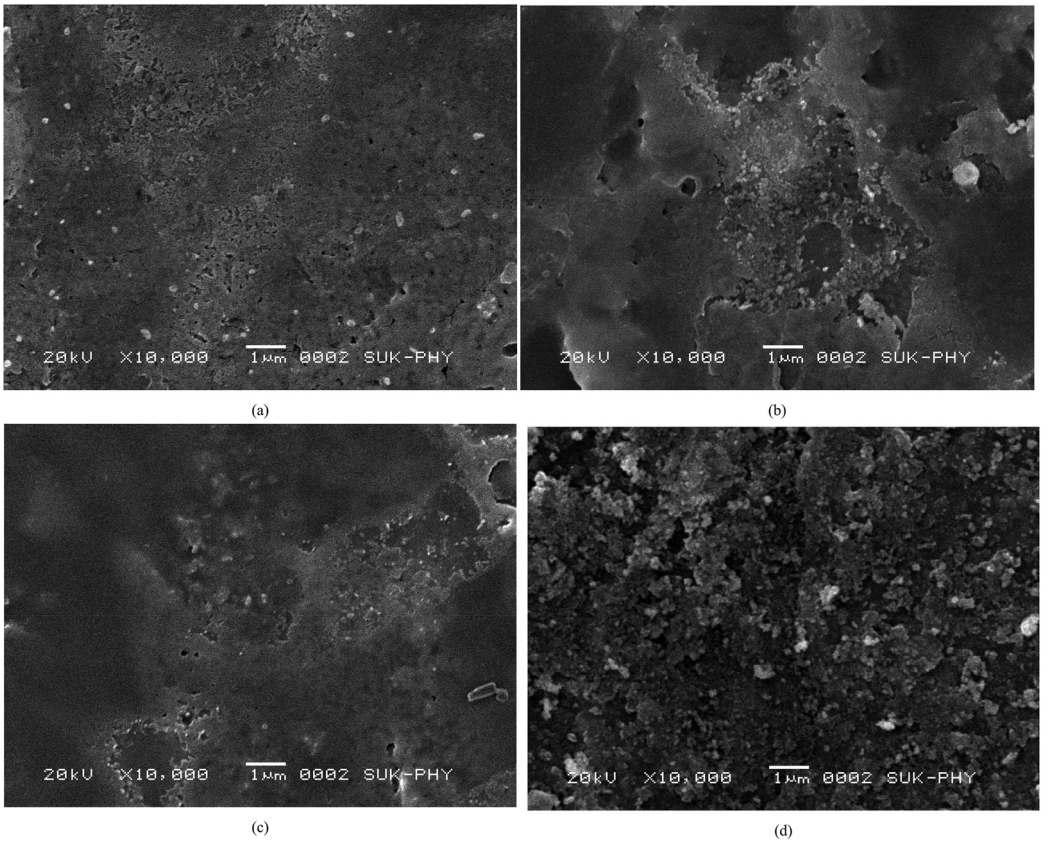

Figure 3. SEM images of Co_3O_4 films spray-deposited with various quantities of the spraying solution (a) 15 cc, (b) 20 cc, (c) 25 cc, and (d) 30 cc.

with smaller size is observed in all the samples and was found to increase with increasing quantity of the spraying solution, with the larger size of grains due to closely packed arrangement of crystallites, which supports XRD results (Figure 2). Increasing the quantity of the spraying solution results in the closure bunching of particles which creates dense morphology, which is attributed to the number of Co_3O_4 molecules in the precursor solution. A similar morphology was also observed by Louardi et al. [28]. The mesoporosity of Co_3O_4 is beneficial for supercapacitor applications.

3.4. Optical studies

The variation of UV-Visible absorption spectra with a wavelength for Co_3O_4 films spray deposited with various quantities of the spraying solution is shown in Figure 4(a). It is observed that up to the wavelength of 800 nm absorbance was high, which indicates a higher absorption in a particular visible spectral region. It gradually decreases in the longer wavelength region. Such behaviour can be due to the internal stress formed by the defects in the structures. Figure 4(b) shows the plots of $(\alpha h\nu)^2$ vs $h\nu$ for Co_3O_4 thin films deposited with different quantities of the spraying solution. From the figure, it is observed that there are two straight line portions in the plots, indicating the existence of two direct allowed band gaps for Co_3O_4 thin films. Optical band gap energies are calculated by the extrapolation of linear portions to the energy axis at $\alpha = 0$. Band gap energy values are in the range of 1.41–1.48 eV for the lower energy region and 1.84–2.02 eV for the higher energy region. Similar results were also reported by Shinde et al. [10] and Patil et al. [29] for cobalt

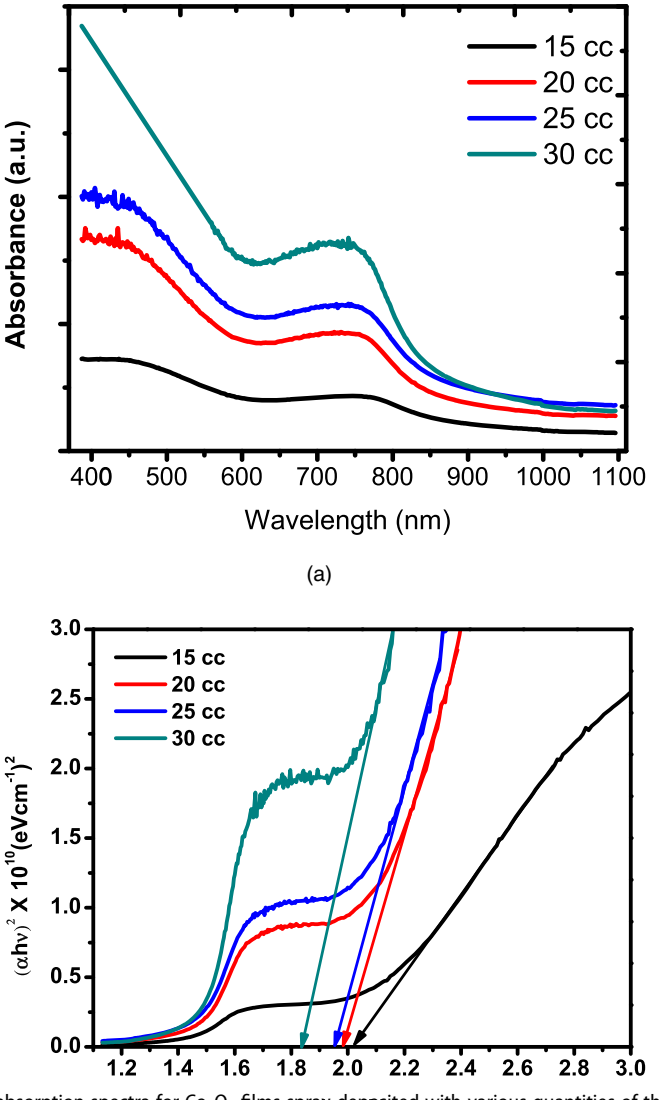

Figure 4. (a) UV-Visible absorption spectra for Co_3O_4 films spray-deposited with various quantities of the spraying solution. (b) Plots of $(ahv)^2$ vs hv for Co_3O_4 films spray-deposited with various quantities of the spraying solution.

oxide thin films. The band gap energy (E_g) varies slightly with the increase in the quantity of the spraying solution. This little shift in band gap energy is attributed to the change in density with variation of quantity of the spraying solution. The shift in absorption edge with increasing quantity of the spraying solution is mainly attributed to the Burstein–Moss effect [30,31]. It was already demonstrated that in semiconductors the absorption edge shifts to smaller wavelength due to the increase in the carrier concentration [32]. This broadening effect in band gap may also be referred to the decrease in the band tail width.

3.5. Electrical resistivity studies

Figure 5 shows the variation of logρ with 1000/T for Co_3O_4 thin films deposited with different quantities of the spraying solution. It is observed that the electrical resistivity decreases with the increase in temperature, showing typical semiconducting behaviour. Room temperature electrical

resistivity of Co_3O_4 thin films is of the order of 10^3 Ω-cm. Electrical resistivity observed in the present study is close to 1.5×10^3 Ω cm reported by Shinde et al. [10] for cobalt oxide thin films. Decrease in film resistivity with the increase in the quantity of the spraying solution is due to the change in grain size and thicker films providing more channels for electron transport.

Activation energy (E_a) is calculated by using the following Arrhenius relation:

$$\rho = \rho_0 exp\left[\frac{E_a}{kT}\right] \tag{3}$$

where ρ is the electrical resistivity at temperature T, ρ_0 is a constant, k is the Boltzmann constant and T is the absolute temperature. Activation energies are in the order of 0.015–0.06 eV, which are close to 0.06–0.08 eV, as observed by Patil et al. [29] for cobalt oxide thin films. Activation energy represents the average energy of the carriers with respect to the Fermi energy, if the carrier can only move at the bottom or top of the well-defined band.

3.6. Electrochemical studies

Previously we studied the influence of substrate temperature on the electrochemical properties of Co_3O_4 thin films [33]. Co_3O_4 nanostructures exhibited good electrochemical performance with excellent cycle stability and high specific capacitance of 425 Fg^{-1} at a scan rate of 5 mVs^{-1}. The electrochemical impedance spectroscopy study indicated that Co_3O_4 nanostructures deposited at 350°C substrate temperature and 15 cc quantity of the spraying solution had better electrochemical properties. To improve the electrochemical performance Co_3O_4 thin films are deposited with different (20, 25 and 30 cc) quantities of the spraying solution.

3.6.1. Cyclic voltammetry

Cyclic voltammetry (CV) curves for Co_3O_4 thin films are measured in 2M aqueous KOH electrolyte in the potential range −0.8 V to +0.1 V. Figure 6(a–d) shows the CV curves at different scan rates. It is observed that as the scan rate raises from 5 to 100 mVs^{-1}, the area under the curve enhances. All curves have a similar nature with pseudo-capacitive behaviour. Analogous results were observed by Kandalkar et al. for electrodeposited Co_3O_4 thin films [34]. Specific capacitance decreases with the rise in scan rate. At lower scan rates, more time is available for diffusion of ions from electrolyte. At

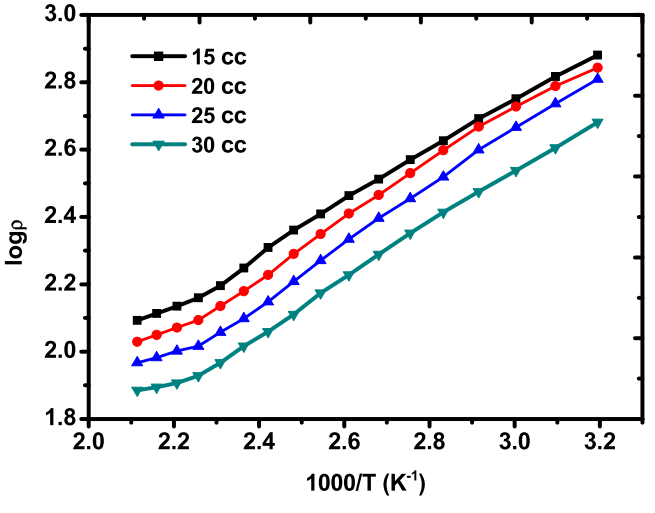

Figure 5. Plots of logρ vs 1000/T for Co_3O_4 films spray-deposited with various quantities of the spraying solution.

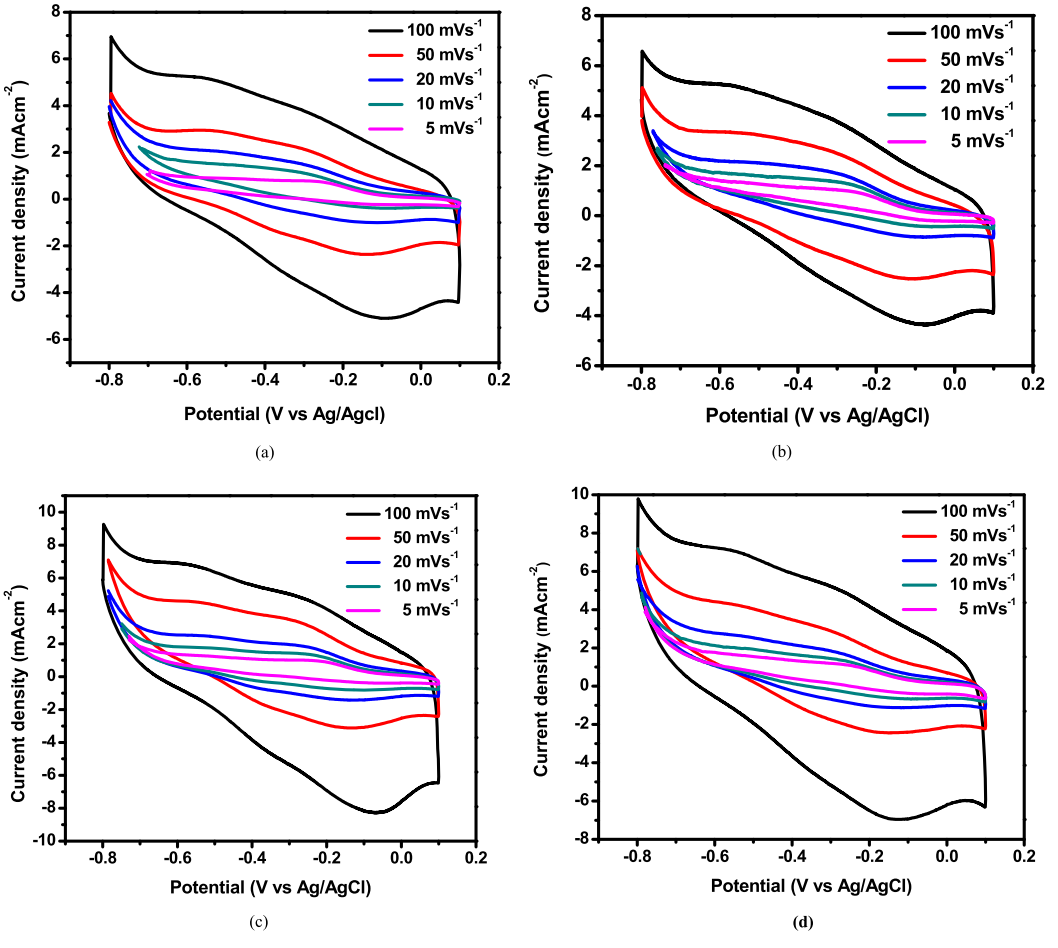

Figure 6. Cyclic voltammograms at different scan rates for Co_3O_4 electrodes spray-deposited with (a) 15 cc, (b) 20 cc, (c) 25 cc and (d) 30 cc of the spraying solution.

higher scan rates, the diffusion effect limits the migration of ions causing some active surface areas to become inaccessible for charge storage [35]. Figure 7(a) shows cyclic voltammograms of Co_3O_4 electrodes in 2M aqueous KOH electrolyte at a scan rate of 10 mVs^{-1}. Specific capacitance (Cs) is calculated by using the following equation [36,37]:

$$C_s = \frac{1}{mv(V_c - V_a)} \int_{V_a}^{V_c} I(V)dV \tag{4}$$

where C_s is the specific capacitance (Fg^{-1}), v is the potential scan rate (mVs^{-1}), I is the current response (mA) of the Co_3O_4 electrode for unit area (1 cm^2) and m is the deposited mass of Co_3O_4 on 1 cm^2 surface of FTO-coated glass substrate. Figure 7(b) shows the variation of specific capacitance with a scan rate in 2M aqueous KOH electrolyte for Co_3O_4 thin film electrodes. From the figure, it is observed that the specific capacitance of 425 Fg^{-1} at 5 mVs^{-1} observed for 15 cc quantity of the spraying solution increases with an increase in the quantity of the spraying solution and reaches maximum 565 Fg^{-1} at 5 mVs^{-1} for Co_3O_4 thin film electrodes deposited with 30cc of quantity of the spraying solution. The Co_3O_4 thin film electrode thickness directly relates to volumetric capacitance. The highest specific capacitance is 565 Fg^{-1} at 5 mVs^{-1}. This value of specific capacitance is better than the values reported in the literature. Kandalkar et al. [34] have reported a

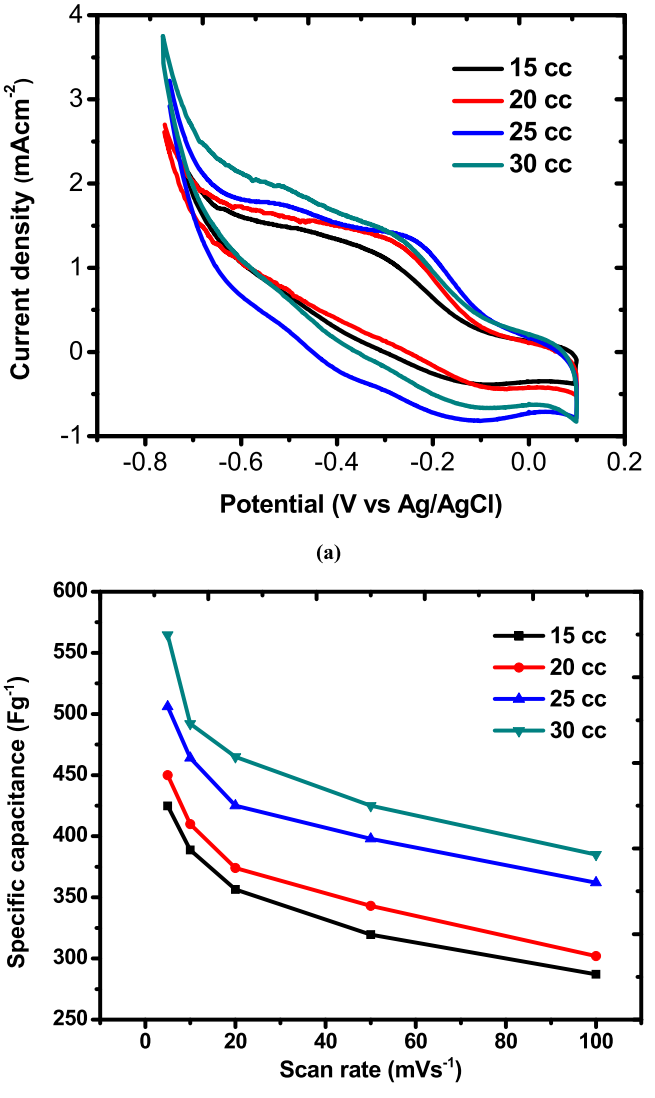

Figure 7. (a) Cyclic voltammograms of Co_3O_4 electrodes in 2M KOH electrolyte at a scan rate of 10 mVs^{-1} spray-deposited with various quantities of the spraying solution. (b) Variation of specific capacitance in 2M KOH electrolyte with a scan rate for Co_3O_4 thin film electrodes spray-deposited with various quantities of the spraying solution.

specific capacitance of 165 Fg^{-1} in 1M KOH. Amabre et al. [38] have reported a specific capacitance of 93.1 Fg^{-1} at 1 mVs^{-1} in 1M KOH electrolyte. Wei Du and coworkers have obtained a specific capacitance of 278 Fg^{-1} for hollow Co_3O_4 boxes [39]. The values of specific capacitance for Co_3O_4 films obtained with various quantities of the spraying solution are given in Table 2.

3.6.2. Galvanostatic charge/discharge

Galvanostatic charge/discharge experiment was done at a current density of 1 Ag^{-1} for Co_3O_4 thin film electrode supercapacitors spray deposited with different quantities of the spraying solution in a stable potential window −0.8 to +0.1 V and the results are shown in Figure 8(a). Specific capacitance (C_{sp}, Fg^{-1}), specific power (SP, $kWkg^{-1}$), specific energy (SE, $Whkg^{-1}$), and coulomb efficiency (η, %) are calculated by using relations given elsewhere [6,40]. Figure 8(b) shows the galvanostatic charge/discharge curves for Co_3O_4 thin film electrode (spray-deposited with 30cc

Table 2. Optical, electrical, electrochemical (cyclic voltammetry) data and R_s and R_{ct} values obtained from Nyquist plot for spray-deposited Co_3O_4 thin films with various quantities of the spraying solution.

Q (cc)	E_{g1} (eV)	E_{g2} (eV)	E_a (eV) L.T.	H.T.	C_s (Fg^{-1})	R_s (Ω)	R_{ct} (Ω cm^2)
15	2.02	1.41	0.015	0.060	425	0.05	12.35
20	1.98	1.43	0.032	0.059	450	0.05	08.56
25	1.96	1.45	0.035	0.052	506	0.04	05.98
30	1.84	1.48	0.036	0.057	565	0.03	04.66

Q: quantity of the spraying solution; E_g: bandgap energy; E_a: activation energy; L.T.: low temperature; H.T.: high temperature; C_s: specific capacitance; R_s: solution resistance; Rct: charge transfer resistance.

quantity of the spraying solution) supercapacitors at different current densities. Specific capacitance was 544 Fg^{-1} at a current density of 1 Ag^{-1}, which decreased to 511 Fg^{-1}, even at the high current density of 4 Ag^{-1}. This value is higher than the value of 304 Fg^{-1} at 0.5 Ag^{-1} recently reported for Co_3O_4 nanoparticle-based electrode [41]. The small initial voltage loss observed from the discharge curves, even at higher current density, demonstrates a fast I-V response and low internal resistance

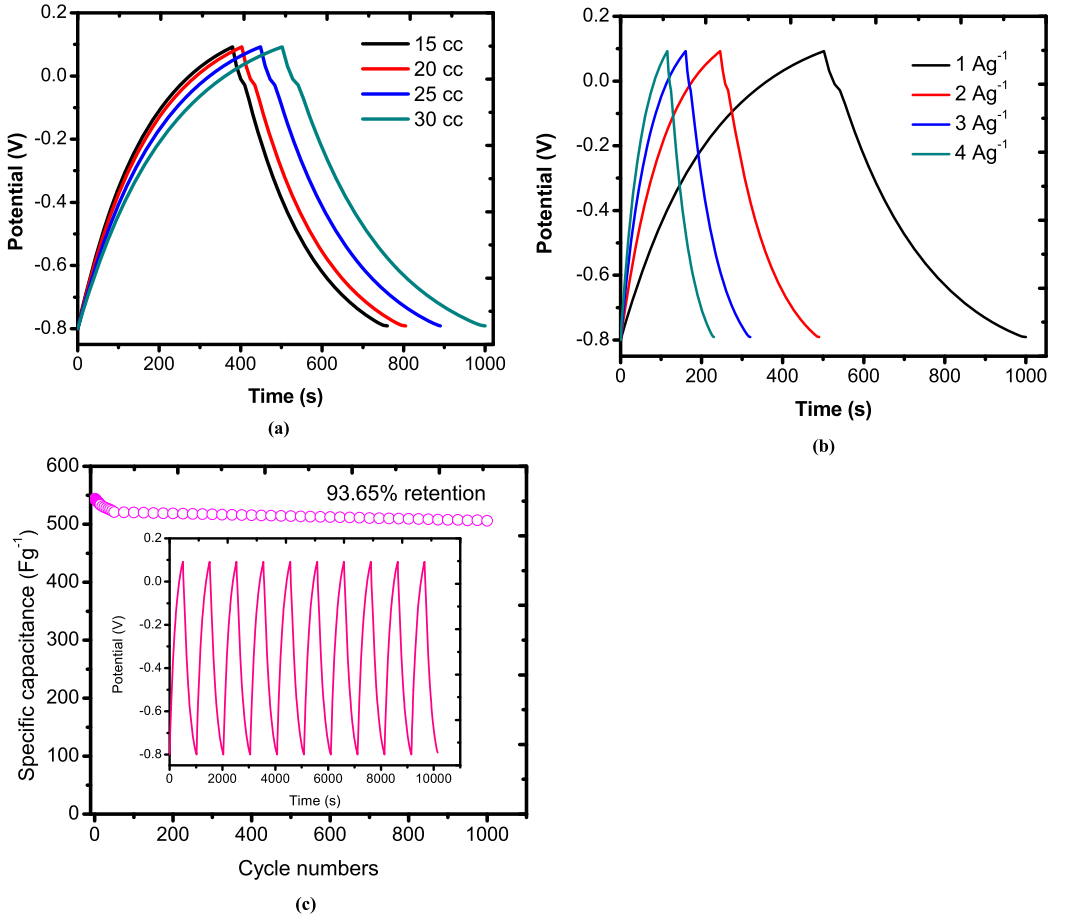

Figure 8. (a) Galvanostatic charge/discharge curves at a current density of 1 $Ag^{-1}$for Co_3O_4 thin film supercapacitors spray-deposited with various quantities of the spraying solution. (b) Galvanostatic charge/discharge curves for Co_3O_4 thin film electrode (spray-deposited with 30 cc quantity of the spraying solution) supercapacitors at different current densities. (c) Long-term cycling performance of the Co_3O_4 film electrode (spray deposited with 30 cc quantity of the spraying solution) at the current density of 1Ag^{-1}. The inset shows the charge–discharge curves of the first 10 cycles of the Co_3O_4 thin film electrode.

Table 3. Various parameters for obtaining specific capacitance, specific energy and specific power from galvanostatic charge/discharge measurements for Co_3O_4 thin films spray-deposited with 30 cc quantity of the spraying solution.

Current density (Ag^{-1})	t_{dis} (s)	C_{sp} Fg^{-1}	SE ($Whkg^{-1}$)	SP (Wkg^{-1})	η (%)
1	490	544	61.25	450	96.08
2	238	529	59.50	900	97.14
3	155	517	58.13	1350	89.60
4	115	511	57.50	1800	89.15

t_{dis}::discharge time; SE: specific energy; SP: specific power; η: coulomb efficiency.

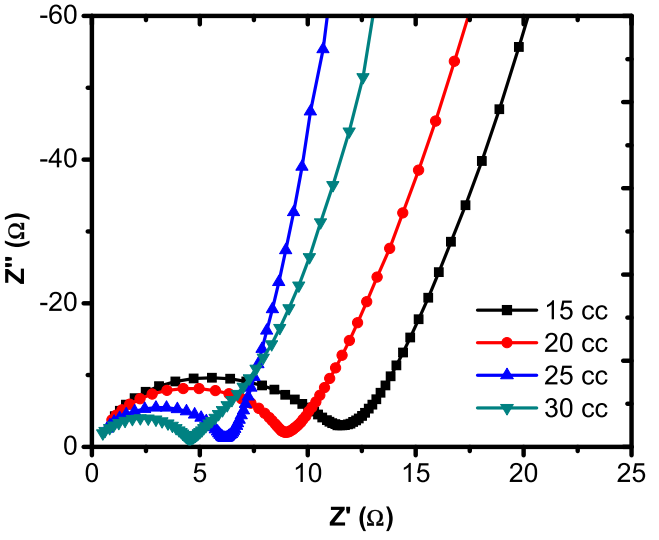

Figure 9. Nyquist plot for Co_3O_4 electrode in 2M KOH electrolyte spray-deposited with various quantities of the spraying solution.

of the supercapacitor [42]. Table 3 shows the values of specific capacitance, specific energy, specific power and coulomb efficiency, respectively obtained from galvanostatic charge/discharge measurements.

Figure 8(c) shows the long-term cycling performance of the Co_3O_4 thin film electrode spray deposited with 30 cc quantity of the spraying solution at the current density of 1 Ag^{-1} for 1000 cycles. Inset displays the charge–discharge curves of the first 10 cycles of the Co_3O_4 thin film electrode. Specific capacitance of the Co_3O_4 electrode maintains 93.65% of its initial value, showing a worthy cycling stability. The 6.35% capacitance loss after 1000 cycles is much better than the 13.5% capacitance loss for as-prepared $Co(OH)_2$ electrodes reported in the literature [43].

3.6.3. Electrochemical impedance spectroscopy

Nyquist plots for Co_3O_4 deposited with various quantities of the spraying solution in 2M aqueous KOH electrolyte are displayed in Figure 9. Intercept of the semicircle to real axis in a high-frequency region contributes to the value of electrolyte resistance (R_s) and the diameter provides the values of charge transfer resistance (R_{ct}) at the interface between electrode and electrolyte [16]. The linear nature of impedance in the low-frequency region represents the diffusion behaviour of ions in the electrode pores. From Figure 9, it is seen that the values of electrolyte resistance (R_s) are around 0.05 Ω and the values of charge transfer resistance (R_{ct}) are given in Table 2.

4. Conclusions

Co_3O_4 thin films are successfully deposited by the spray pyrolysis technique with different quantities of the spraying solution. Film thickness increases with an increase in the quantity of the spraying solution. Co_3O_4 has a cubic crystal structure with lattice parameter a = b = c = 8.030 Å. A mesoporous structure is observed in the SEM analysis. Electrical resistivity decreases as quantities of the spraying solution increase. Optical band gap values are 1.41–1.48 eV in the lower energy region and 1.84–2.02 eV for the higher energy region. Specific capacitance of 565 Fg^{-1} is calculated from cyclic voltammetry. Specific capacitance of the Co_3O_4 electrode retains 93.65% of its initial value after 1000 cycles, showing a worthy cycling stability. Also, the electrochemical impedance spectroscopy showed that mesoporous electrodes lower the charge transfer resistance up to 4.66 Ω-cm^2. The remarkable mesoporous structure and electrical resistivity enable Co_3O_4 electrodes to be the promising electrode materials for the next-generation high-performance supercapacitors.

Acknowledgements

Dr. A. A. Yadav is grateful to the Science and Engineering Research Board, Department of Science and Technology, New Delhi, India for the financial assistance through the Project under the SERC Fast Track Scheme for Young Scientist (File No. SB/FTP/PS-068/2013).

Disclosure statement

No potential conflict of interest was reported by the author(s).

Funding

This work was supported by Science and Engineering Research Board, Department of Science and Technology, New Delhi, India [grant number: SERC Fast Track Scheme for Young Scientist File No. SB/FTP/PS-068/2013].

ORCID

Abhijit A. Yadav http://orcid.org/0000-0002-3486-4099

References

[1] Messaoudi O, Mansouri M, Manai L, et al. Spectroscopic ellipsometry investigation and morphological characterization of electrodeposited Cu_2O thin films: annealing effect. Phase Transitions. 2020;93(12):1171–1182.
[2] Messaoudi O, Elgharbi S, Bougoffa A, et al. Annealing temperature investigation on electrodeposited Cu_2O properties. Phase Transitions. 2020;93(10–11):1089–1099.
[3] Yadav AA. SnO_2 thin film electrodes deposited by spray pyrolysis for electrochemical supercapacitor applications. J. Mater. Sci.: Mater. Electron. 2016;27:1866–1872.
[4] Henry J, Daniel T, Balasubramanian V, et al. Electrical and optical properties of Sb-doped Cu_2Se thin films deposited by chemical bath deposition. Phase Transitions. 2020;93(8):793–801.
[5] Klaa K, Labidi S, Bououdina M, et al. Temperature and pressure dependence on structural, electronic and thermal properties of ZnO wurtzite phase-first principle investigation. Phase Transitions. 2020;93(7):654–665.
[6] Conway BE. Electrochemical supercapacitors: scientific fundamentals and technological applications. New York (NY): Kluwer Academic/Plenum Publishers; 1999.
[7] Ke Q, Wang J. Graphene-based materials for supercapacitor electrodes – a review. J. Materiomics. 2016;2:37–54.
[8] Wang N, Zhao P, Liang K, et al. CVD-grown polypyrrole nanofilms on highly mesoporous structure MnO_2 for high performance asymmetric supercapacitors. Chem. Engg. J. 2017;307:105–112.
[9] González A, Goikolea E, Barrena JA, et al. Review on supercapacitors: technologies and materials. Renew. Sustain. Energy Rev. 2016;58:1189–1206.
[10] Shinde VR, Mahadik SB, Gujar TP, et al. Supercapacitive cobalt oxide (Co_3O_4) thin films by spray pyrolysis. Appl. Surf. Sci. 2006;252:7487–7492.

[11] Deng J, Feng S, Zhang K, et al. Heterogeneous activation of peroxymonosulfate using ordered mesoporous Co_3O_4 for the degradation of chloramphenicol at neutral pH. Chem. Engg. J. 2017;308:505–515.
[12] Patil V, Joshi P, Chougule M, et al. Synthesis and characterization of Co_3O_4 thin film. Soft Nanosci. Lett. 2012;2:1–7.
[13] Pal M, Rakshit R, Singh AK, et al. Ultra high supercapacitance of ultra-small Co_3O_4 nanocubes. Energy. 2016;103:481–486.
[14] Kim H-K, Seong T-Y, Lim JH, et al. Electrochemical and structural properties of radio frequency sputtered cobalt oxide electrodes for thin-film supercapacitors. J Power Sources. 2011;102:167–171.
[15] Huang G, Xu S, Lu S, et al. Porous polyhedral and fusiform Co_3O_4 anode materials for high-performance lithium-ion batteries. Electrochim Acta. 2014;135:420–427.
[16] Jagadale AD, Kumbhar VS, Lokhande CD. Supercapacitive activities of potentiodynamically deposited nanoflakes of cobalt oxide (Co_3O_4) thin film electrode. J. Coll. Inter. Sci. 2013;406:225–230.
[17] Jiang Y, Chen L, Zhang H, et al. Two-dimensional Co_3O_4 thin sheets assembled by 3D interconnected nanoflake array framework structures with enhanced supercapacitor performance derived from coordination complexes. Chem. Engg. J. 2016;292:1–12.
[18] Guan B, Li Y, Yin B, et al. Synthesis of hierarchical NiS microflowers for high performance asymmertric supercapacitor. Chem. Engg. J. 2017;308:1165–1173.
[19] Salunkhe RR, Jang K, Yu H, et al. Chemical synthesis and electrochemical analysis of nickel cobaltite nanostructures for supercapacitor applications. J. Alloys Comp. 2011;509:6677–6682.
[20] Jagadale AD, Kumbhar VS, Bulakhe RN, et al. Influence of electrodeposition modes on the supercapacitive performance of Co_3O_4 electrodes. Energy. 2014;64:234–241.
[21] Tang W, Yao M, Deng Y, et al. Decoration of one-dimensional MnO_2 with Co_3O_4 nanoparticles: A heterogeneous interface for remarkably promoting catalytic oxidation activity. Chem. Engg. J. 2016;306:709–718.
[22] Yadav AA, Barote MA, Dongre PM, et al. Studies on growth and characterization of $CdS_{1-x}Se_x$ ($0.0 \leq x \leq 1.0$) alloy thin films by spray pyrolysis. J. Alloys Comp. 2010;493:179–185.
[23] Yadav AA, Masumdar EU, Moholkar AV, et al. Effect of quantity of spraying solution on the properties of spray deposited fluorine doped tin oxide thin films. Physica B. 2009;404:1874–1877.
[24] JCPDS data card 76–1802.
[25] Patil NM, Nilange SG, Jundale VA, et al. Structural, optical and electrical properties of spray-deposited Fe-doped nanocrystalline $ZnS_{0.2}Se_{0.8}$ thin films. Phase Transitions. 2021;94(6–8):493–510.
[26] Manickam M, Ponnuswamy V, Sankar C, et al. Cobalt oxide thin films prepared by NSP technique: impact of molar concentration on the structural, optical, morphological and electrical properties. Optik. 2016;127:5278–5284.
[27] Giraldi TR, Escote MT, Bernardi MIB, et al. Effect of thickness on the electrical and optical properties of Sb doped SnO_2 (ATO) thin films. J Electrocera. 2004;13:159–165.
[28] Louardi A, Rmili A, Ouachtari F, et al. Characterization of cobalt oxide thin films prepared by a facile spray pyrolysis technique using perfume atomizer. J. Alloys Comp. 2011;509:9183–9189.
[29] Patil PS, Kadam LD, Lokhande CD. Preparation and characterization of spray pyrolysed cobalt oxide thin films. Thin Solid Films. 1996;272:29–32.
[30] Burstein E. Anomalous optical absorption limit in InSb. Phys. Rev. 1954;93:632–633.
[31] Moss TS. The interpretation of the properties of indium antimonide. Proc. Phys. Soc. Lond. 1954;B67:775.
[32] Lee GH, Yamamoto Y, Kourogi M, et al. Blue shift in room temperature photoluminescence from photochemical vapor deposited ZnO films. Thin Solid Films. 2001;386:117–120.
[33] Yadav AA, Chavan UJ. Electrochemical supercapacitive performance of spray deposited Co_3O_4 thin film nanostructures. Electrochim Acta. 2017;232:370–376.
[34] Kandalkar SG, Lee H-M, Chae H, et al. Structural, morphological, and electrical characteristics of the electrodeposited cobalt oxide electrode for supercapacitor applications. Mater. Res. Bull. 2011;46:48–51.
[35] Dubal DP, Jagadale AD, Patil SV, et al. Simple route for the synthesis of supercapacitive Co–Ni mixed hydroxide thin films. Mater. Res. Bull. 2012;47:1239–1245.
[36] Yadav AA, Jadhav SN, Chougule DM, et al. Spray deposited hausmannite Mn_3O_4 thin films using aqueous/organic solvent mixture for supercapacitor applications. Electrochim Acta. 2016;206:134–142.
[37] Yadav AA. Influence of electrode mass-loading on the properties of spray deposited Mn_3O_4 thin films for electrochemical supercapacitors. Thin Solid Films. 2016;608:88–96.
[38] Ambare RC, Bharadwaj SR, Lokhande BJ. Nonaqueous media dependent scientific supercapacitive measurements of Co_3O_4 thin film electrodes prepared by spray pyrolysis. Inter. J. Sci. Nat. 2014;5:663–668.
[39] Du W, Liu R, Jiang Y, et al. Facile synthesis of hollow Co_3O_4 boxes for high capacity supercapacitor. J Power Sources. 2013;227:101–105.
[40] Salunkhe RR, Lin J, Malgras V, et al. Large-scale synthesis of coaxial carbon nanotube/$Ni(OH)_2$ composites for asymmetric supercapacitor application. Nano Energy. 2015;11:211–218.
[41] Li Z-Y, Bui PTM, Kwak D-H, et al. Enhanced electrochemical activity of low temperature solution process synthesized Co_3O_4 nanoparticles for pseudo-supercapacitors applications. Ceram. Inter. 2016;42:1879–1885.

[42] Salunkhe RR, Tang J, Kamachi Y, et al. Asymmetric supercapacitors using 3D nanoporous carbon and cobalt oxide electrodes synthesized from a single metal–organic framework. ACS Nano. 2015;9:6288–6296.
[43] Qiu K, Lu Y, Cheng J, et al. Ultrathin mesoporous Co_3O_4 nanosheets on Ni foam for high-performance supercapacitors. Electrochim Acta. 2015;157:62–68.